Title

Structural Stability of Iodide Perovskite: A Combined Cluster Expansion Method and First-Principles Study

Authors

K. Yamamoto, S. Iikubo*, J. Yamasaki, Y. Ogomi, and S. Hayase

Graduate School of Life Science and Systems Engineering, Kyushu Institute of Technology, Kitakyushu 808-0196, Japan

Email: iikubo@life.kyutech.ac.jp

Abstract

To aid the development of Pb-free perovskite solar cells, the stability of the iodide perovskite structure ABI_3 has been investigated by first-principles calculations, Bader charge analysis, and the cluster expansion method. At the A sites, methylammonium (MA, $CH_3NH_3^+$), formamidinium (FA, $CH(NH_2)_2^+$), and Cs^+ were modeled, while at the B sites, one or two elements from Pb, Sn, Ge, In, Ga, Bi, and Sr were examined. For the partially substituted system $A(B,B')I_3$, we found that the stability strongly depends on the identity of the A-site cation. For example, $Cs(B,B')I_3$ structures are stabilized by a mixture of divalent cations, such as Pb, Sn, and Ge, at the B site. Concerning the stabilization mechanisms, Coulomb energy gain seems to be the origin of the structural stability in A = Cs structures. From our results, $Cs(B,B')I_3$, where the B site is occupied by divalent cations, are possible candidates for high stability, lead-free solar cell materials.

Introduction

As generators of renewable energy, solar cells are very attractive devices, and these are being developed for the realization of a sustainable low-carbon society. Recently, an organic–inorganic hybrid perovskite solar cell was reported by Miyasaka *et al.*[1]. In this cell, the conversion efficiency reached 22.1%[2], and this value is similar to those of silicon-based solar cells, which are, currently, the most popular type of solar cell. Therefore, perovskite-based devices are expected to be the next generation of solar cells. In this type of solar cell, the iodide perovskite compound $CH_3NH_3PbI_3$ is used as the light absorbing layer. This material has a long carrier life, and this is one of the reasons for its photoelectric conversion properties. Furthermore, the fabrication of this solar cell is easy via a printing method, allowing low-cost production.

The chemical formula of the perovskite type crystal structure can be represented as ABX_3. Figure 1 shows the crystal structure of (a) perovskite-type $CsPbI_3$ and (b) and (c) show the structures of CH_3NH_3 and $CH(NH_2)_2$, respectively In the $CH_3NH_3PbI_3$ perovskite, the A, B, and X sites are occupied by organic methylammonium (MA, $CH_3NH_3^+$), Pb, and I, respectively. For the practical use of perovskite solar cells, the use of lead, which is toxic, will become a serious issue. Another problem is in the relatively low stability of the crystal structure of $CH_3NH_3PbI_3$, and there have been several reports that perovskite compounds with organic molecule are unstable in the presence of moisture, oxygen, light, and heat[3—5]. Therefore, the improvement in the stability of the crystal structure is a critical issue.

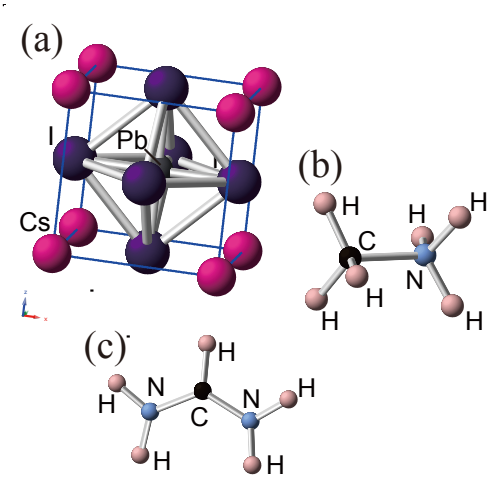

Figure 1. (a) Crystal structure of the iodide perovskite $CsPbI_3$ and two ABI_3 A-site molecules (b) $CH_3NH_3^+$ (MA) and (c) $CH(NH_2)_2^+$ (FA).

To solve these issues, the search for lead-free and highly stable perovskite materials has been conducted both theoretically and experimentally. Recently, first-principles calculations have become one of the most attractive calculation tools in the search for new materials. For lead-free iodide perovskites, $MASnI_3$, $CsSnI_3$, $MASrI_3$, $MABiSI_2$, $MABi_{0.5}Tl_{0.5}I_3$, and $MACaI_3$ have been suggested to be promising candidates by first-principles calculation[6—12]. The electronic structures and band gaps have also been investigated by this calculation technique. In addition, several chalcogenides, such as $CaTiS_3$ and $CaZrSe_3$, have also been investigated as possible photovoltaic materials[13]. In addition, the A-site dependence[14,15], double perovskite structure[16—19], and the halogen-site substitution effects on the stability and band gap have been investigated for I, Br, and Cl[20]. For the investigation of bulk alloy systems, an algorithm has been developed that has been highly successful at finding the most likely ground state configuration. The algorithm is based on a cluster expansion of the energy of an alloy[21—25] and can consider many more structures than a straightforward trial and error search by ab-initio calculation.

In this study, we focused on the search for the lead-free or lower-lead-content iodide perovskite compounds. Thus, the stabilities of iodide perovskite compounds where Pb is fully substituted or partially substituted by other cations have been investigated. As described above, X-site substituted system were studied by Yin *et al.*[20],

but B-site partially substituted systems have not been studied before in the extended composition region, except for ordered double perovskite systems[16—19]. Therefore, we examined the stabilities of iodide perovskites with ABI_3 structures constructed by replacing Pb^{2+} with other ions. For partially substituted system, we employed the cluster expansion method (CEM) to find the ground state of the $A(B,B')I_3$ solid solution. For the A sites, two kinds of organic molecules, MA and $CH(NH_2)_2^+$ (FA), and one inorganic ion, Cs^+, were considered. We found that the stability of the partially substituted system $A(B,B')I_3$ is strongly dependent on the identity of the A-site ion. $Cs(B,B')I_3$ is stabilized by a mixture of divalent cations, such as Pb, Sn, and Ge. On the other hand, $MA(B,B')I_3$ and $FA(B,B')I_3$ are stabilized in the In-Sn and In-Bi systems. To discuss the microscopic mechanism of the role of A-site ions on the structural stability, we have studied the electronic and bonding states between each site. The oxidation state of each ion was evaluated by Bader charge analysis, and the Coulomb energy gain expected in the partially substituted system is discussed as a possible mechanism for the stabilization of $Cs(B,B')I_3$.

Computational methods

In this study, the fully substituted structure ABI_3 and the partially substituted structure $A(B,B')I_3$ were investigated. The latter system is more complex than the former because it has many configurational degrees of freedom, even at a fixed composition. Among the many configurations, the most stable structures were determined by the cluster expansion method[22,23] combined with first-principles calculations.

The cluster expansion of the energy is given simply by

$$E = \sum_{\alpha} J_{\alpha} \xi_{\alpha} \quad , \tag{1}$$

where E is the energy per site in the structure. The cluster correlations, ξ_{α}, are expressed as products of the occupants of the sites that make up cluster α. The sum runs over clusters α, and J_{α} is the effective cluster interaction (ECI) associated with the cluster. Note that, while the ECIs are generally unknown, the energies of the structures can be computed using first-principles methods such as density functional electronic structure methods. Once energies for a set of structures have been obtained, the ECIs can be obtained by inverting the cluster expansion, provided that the summation over clusters can be truncated. Importantly, now that approximate ECIs are known, the energy of any structure can be predicted using the cluster expansion. This easy computation of energies from ECIs and ECIs from energies is at the heart of the cluster expansion algorithm for ground-state searching.

The many ordered structures of different compositions were constructed on the lattice of each phase by using the "Alloy Theoretic Automated Toolkit" (ATAT) code[21]. The total energy calculations were performed using the Vienna ab initio program (VASP) code[26,27], which is based on density functional theory. The exchange and correlation functions were given by the generalized gradient approximation, as proposed by Perdew *et al.*[28]. We employed Blöchl's projector-augmented wave (PAW) method as implemented by Kresse and Joubert[29]. The details of the first-principles calculations conducted in ATAT are as follows. The plane wave energy cutoff was chosen to be 400 eV to ensure lattice relaxation. The k-point meshes were created with k-points per reciprocal atom of 1000. The first-order Methfessel–Paxton method was used for the Fermi surface with a sigma value as small as 0.2 eV. The convergence criterion was set to a 10^{-4} eV change in the energy during the geometry optimization iterations. The cell volume, shape, and atomic positions were allowed to relax until the stress was minimized and the forces on any atom were less than 0.02 eV/Å. For the total energy calculation of fully substituted

structures, the k-point meshes were created with 0.15 /Å. Therefore, the size of the k mesh depends on the crystal structure. For example, we used 7 × 7 × 7 meshes for the calculations of 1 × 1 × 1 cubic perovskite unit cell. Formation energies are evaluated using fully relax structures in terms of the cell volume, shape, and atomic positions.

Bader charge analysis was performed to estimate the charge state of individual atoms in the perovskite structure[30]. From the charge density distribution obtained from the first-principles calculations, the charge belonging to each atom was estimated. The total charge density was separated at the minimum points from the maximum at the center of the atom. Because the position of maximum charge density is slightly offset from the atomic center when using the pseudopotential method employed in VASP, a correction for the deviation was carried out. For the analysis, codes developed by the Henkelman group were used.

Results and discussion

Before discussing the partially substituted system, we discuss the results for the fully substituted system to understand the basic stabilization mechanism of the iodide perovskite structure. The formation energies for the fully substituted ABX_3-type perovskites, where A = MA, FA, and Cs and B = Sn, Ge, In, Ga, Bi, and Sr, were evaluated. First total energies of ABX_3 were calculated for the fully relaxed structures from the cubic, tetragonal, and orthorhombic initial crystal structures (For A = FA, only cubic initial structure was examined for the simplicity). These calculated results are summarized in Supporting Information, Table S1. Among of them, the lowest energies, which is denoted by shading in the table were used as the total energy of each ABI_3 $E(ABI_3)$. The formation energies ΔE were evaluated in two different ways. One is the estimation using pure substances (bulk stable structure) as a reference state, as defined by Eq. (2).

$$\Delta E_1 = E(ABI_3) - E(A) - E(B) - 3 \times E(I) \quad (2)$$

The first term on the right-hand side is the total energy of ABI_3, the second term is the total energy of A that consists of an A atom, the third term is the total energy of a phase that consists of a B atom, and the fourth term is the total energy of I for the orthorhombic phase (space group *Cmca*) that consists of three atoms. When the organic molecules MA and FA were used, $E(A)$ was calculated from the formation energies of the diamond allotrope of carbon and molecular hydrogen and oxygen.

As an another way, the formation energies of ABX_3 perovskites were evaluated by using the stable iodide compounds as reference states. This estimation is important because it yields information on possible decomposition reactions of the ABX_3 perovskites. The formation energies, ΔE, are defined by Eq. (3).

$$\Delta E_2 = E(ABI_3) - E(AI) - E(BI_2) \quad (3)$$

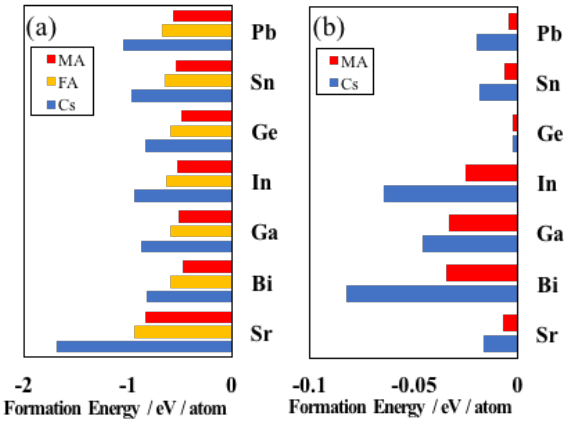

Figure 2. Formation energy for ABI_3. (a) The reference states are the pure elements with bulk stable structure. (b) The reference states are the stable compounds used for synthesis.

Figure 2(a) shows the calculated formation energies, which were estimated with the pure elements with bulk stable structure as reference states. For all compounds, the formation energies are negative, indicating stable or metastable structures. In particular, $CsSrI_3$ shows the very high stability typical of the perovskite structure. For perovskites containing the same family of elements in the periodic table, the formation energy became large and negative with increasing atomic number. On the other hand, stable structures were obtained for A = Cs, FA, and MA in descending order. As shown in Figure 1, there are several possible reasons for the origin of A ion dependence, such as size, shape and their polarity. The inorganic ions are almost spherical in shape; in contrast, FA has planar structure with an inversion center, whereas MA has a non-planar structure without an inversion center, which brings about polarity. The dependence of the structural stability on the identity of the A-site ions should be understand to consider their difference and revealed in the future work. Experimental studies have revealed that MA stabilizes the perovskite structure to a greater degree than FA when B = Pb[31]. On the other hand, other results have suggested that compounds with A = FA are more stable than those with MA in the presence of the heat and moisture in the air[32]. Furthermore, the compound with A = Cs is more thermally stable rather than that with A = MA[33]. These experimental results are consistent with our calculated results.

Figure 2(b) shows the calculated formation energies, which were estimated using the stable iodide compound as a reference state. Chemical reactions proceed from high

energy to low energy states because of the driving force estimated from the energy difference between the free energies of products and reactants. Therefore, this estimation is important because it tells us the possibility of decomposition reactions of ABX_3. In the all case, the formation energies were negative, suggesting that the crystal structures are stable. Among of them, stability of the iodide perovskite compounds with Pb, Sr and Ge are relatively low. This result is due to the high stability of the starting material, PbI_2, SnI_2, and GeI_2. Thus, these systems may undergo decomposition from $APbI_3$ to AI and BI_2 in the external condition, such as heat, atmosphere, and defects.

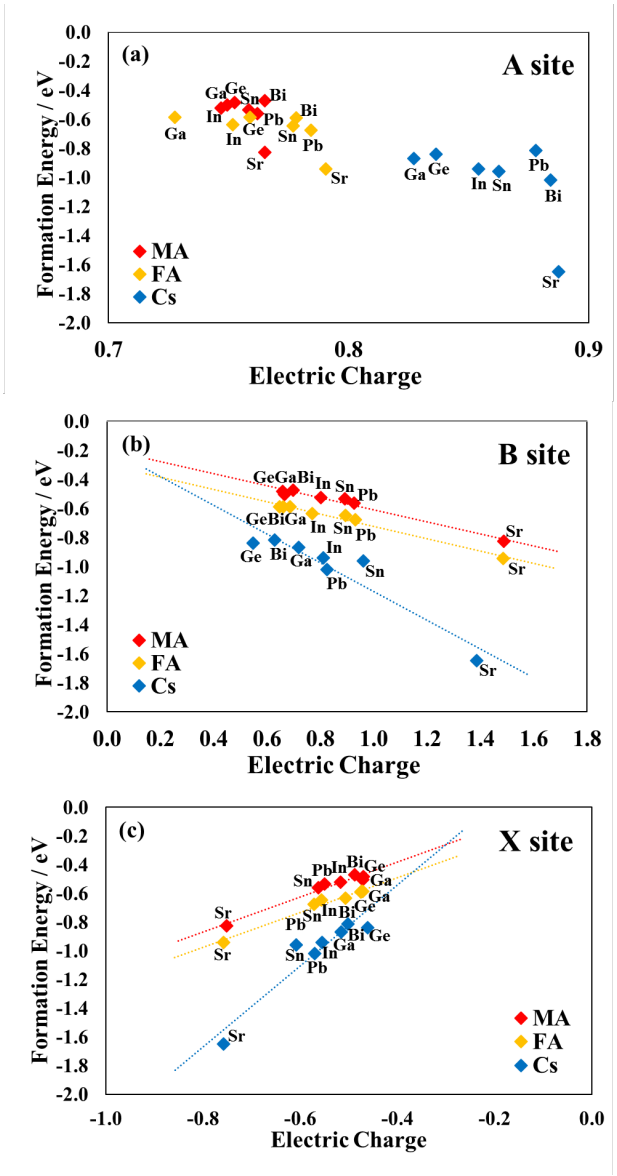

Figure 3. The correlation between the formation energies of the perovskite compounds and the electric charge at (a) A, (b) B, and (c) X sites.

The main contribution to the negative formation energy in the perovskite compounds is the ionic bonding. Thus, the charge at the A, B, and X sites was evaluated by Bader charge analysis, and the correlation between the formation energy and electric charge at each site was analyzed. Figure 3(a)–(c) show the correlation between the charge at each site and the formation energy.

As shown in the figure, there is a strong correlation between the electric charge and the formation energy for all sites. With increasing charge, the formation energy

decreases, suggesting that the ionic bonding stabilizes the perovskite structure. This correlation, however, is relatively weak for the A site, as shown in Figure 3(a). The charge at the A-site varies from about 0.75 to 0.9, and the highest charge value is observed for Cs at 0.8 to 0.9, although it is about 0.75 for MA and FA. This result shows that strong ionic bonding is expected for the compounds containing Cs. On the other hand, the formation energies show a strong electric charge dependence for the B and X sites compared to the A site, as shown in Figs. 3(b) and (c). For both B and X sites, three lines are seen, corresponding to the results for Cs, MA, and FA, and each line has a different slope. At the B site, the electric charge strongly depends on the B-site elements. At the X site, the charge on iodide also depends on the B-site elements. These results strongly suggest the importance of ionic bonding for the stabilization of the iodide perovskites.

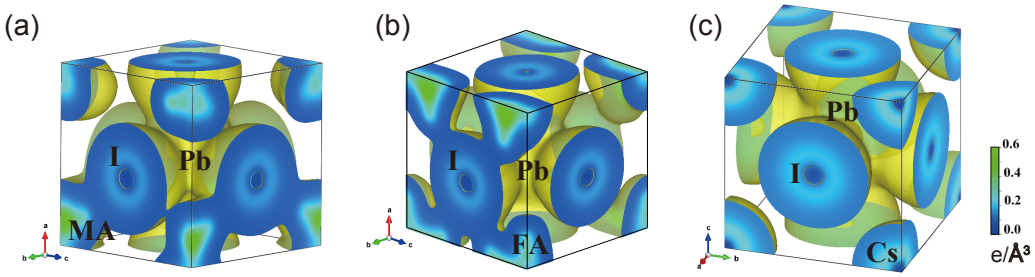

Figure **4**. Visualization of the charge density calculated by first-principles calculations for (a) $MAPbI_3$, (b) $FAPbI_3$, and (c) $CsPbI_3$.

Although a relatively weak correlation between the formation energies and the electric charge is observed at the A site, the A-site ion does contribute to the structural stability; for example, compounds containing Cs are more stable than those containing MA and FA. These differences were examined by visualizing the charge densities of $MAPbI_3$, $FAPbI_3$, and $CsPbI_3$, as shown in Figure 4(a)–(c), respectively. In this figure, a yellow surface indicates an equivalent charge surface of 0.005 e/Å^3, and blue colored regions indicate a charge density greater than 0.005 e/Å^3. As shown in the figures, there is a finite electron distribution associated with covalent bonding between the B site and I site for the three structures. On the other hand, the electron distribution between the A and I sites varies with the identity of the ion at the A site. For MA and FA, there is a distribution of electrons between A and I sites, connecting the two sites by electron transfer. This electronic connection results in a high charge density in between MA-I and FA-I, suggesting covalent

bonding. On the other hand, in $CsPbI_3$, the charge density between Cs and I is low, and Cs does not share electrons with other sites. This indicates strong ionic bonding between Cs-I. The charge densities at the middle points between A and I were quantitatively estimated to be 0.02 e/Å^3 for $MAPbI_3$ and $FAPbI_3$ and ~0.003 e/Å^3 for $CsPbI_3$. The charge distribution between A and I for the organic molecules are five times greater than that of the inorganic Cs^+ ion. This difference is also observed in the systems with B = In, Sn, and Bi. We conclude that the MA-I and FA-I covalent bonding and the Cs–I ionic bonding is, in general, independent of the identity of the B-site cation in the iodide perovskites.

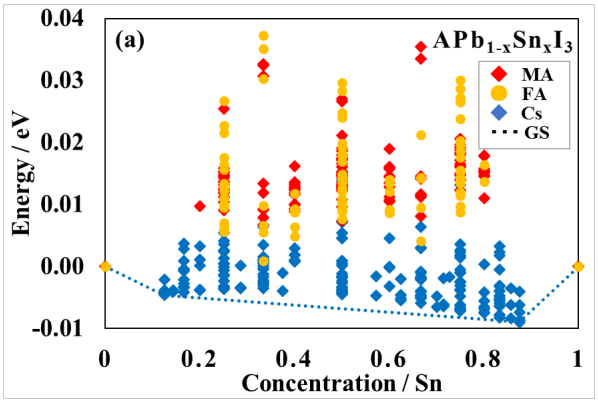

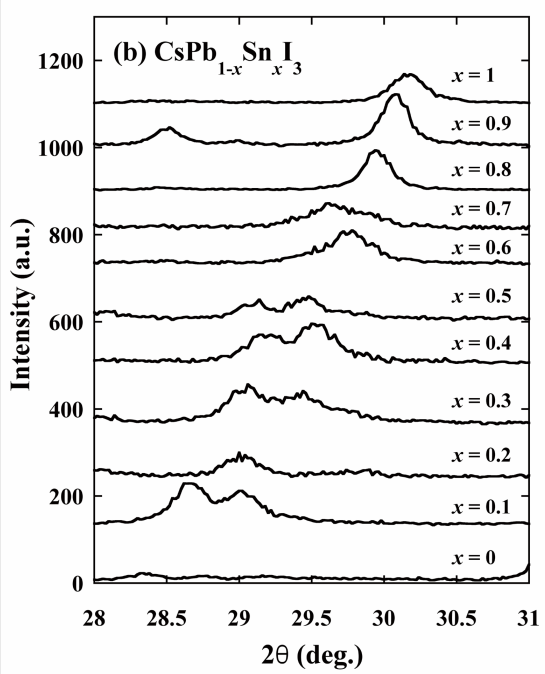

Figure 5. (a) The results of the ground state search performed using the CEM in $APb_{1-x}SnI_3$. (b) XRD patterns of $CsPb_{1-x}Sn_xI_3$ in $28° < 2\theta < 31°$.

In terms of the ionic bonding, the structure is stabilized when A is a monovalent cation, B is a divalent cation, and X is a monovalent anion. We examined the possibility of the partial substitution of Pb by other divalent cations. First, the formation energies of symmetry-nonequivalent structures in $APb_{1-x}Sn_xI_3$ were calculated based on CEM for up to 84, 84, and 40 atoms per supercell for A = MA, FA, and Cs, respectively. Figure 5(a) shows the result of CEM, where red, orange, and blue marks correspond to the results with A = MA, FA, and Cs, respectively. To

estimate the energy variation arising from the ion mixing at the B site, the formation energies of each ordered structures were evaluated with $APbI_3$ and $ASnI_3$ as reference states. As shown in Figure 5(a), all the structures with A = MA and FA have positive formation energies, and several structures containing FA have lower energies than those with MA. This result indicates the instabilities of the mixed states in the MA and FA systems. Because the structures with ordered Pb and Sn arrangement are higher than the averaged value of $APbI_3$ and $ASnI_3$. This result can be considered as a consequence of the relative weak attractive interaction between Pb and Sn at the B sites, because Pb and Sn goes to be separated. On the other hand, many structures with negative formation energies were confirmed for A = Cs, and this arises from the relative strong attractive interaction between Pb and Sn at the B sites. This B-site interaction results in the stabilization of the perovskite structure. Here, we focus on the results for the A = Cs structure in more detail. The formation energies for $x = 0.5$ are located above the curved dashed line, which indicates the ground state. This means that the system with $x \approx 0.5$ is unstable with respect to phase separation. From the calculated result, the system seems to be stabilized against phase separation between $x \approx 0.125$ and 0.875, even at $T = 0$. The obtained stable structures at $x = 0.125$ and 0.875 are given in Supporting Information, Table S2 and Figure S3.

This predicted phase separation tendency in $CsPb_{1-x}Sn_xI_3$ was confirmed by experiment. Figure 5(b) shows the intensity of the (200) diffraction peak of $CsPb_{1-x}Sn_xI_3$ as determined by X-ray diffraction measurements. As x increases, the (200) peak shifts to higher angle, indicating that Pb in $CsPbI_3$ is replaced by Sn, forming a solid solution. Concerning the (200) peak, a double peak structure was observed for $x = 0.1$ and 0.3–0.7. This peak structure can be explained by the coexistence of two perovskite phases with different lattice parameters. In this concentration region, two types of $CsPb_{1-x}Sn_xI_3$, where one is Pb-rich and another is Sn-rich, exist in our sample. The experimental results are consistent with our theoretical predictions, which show the trend in the phase separation behavior. Here, we would like to point out the possibility if the phase separation occurs in nano-scale, a conversion efficiency becomes high, as discussed in ref. 34. Such nano-scale phase separation can be formed due to the spinodal decomposition, which is spontaneous phase separation without an interface between two phases. As revealed in the following section, the phase separation tendency on the B site is observed in many systems. This property can be potentially important factor for high conversion efficiency.

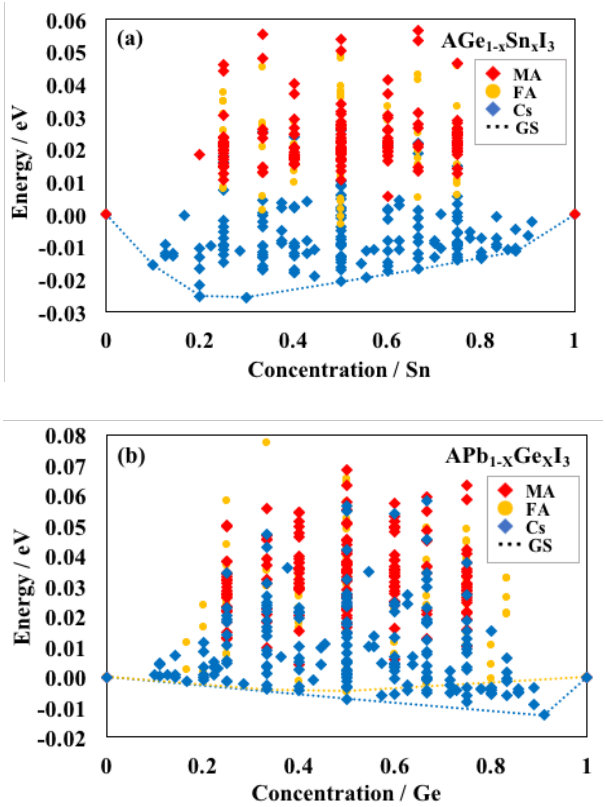

Figure 6. The results of the ground state search performed using the CEM in (a) $AGe_{1-x}Sn_xI_3$ and (b) $APb_{1-x}Ge_xI_3$.

Figure 6(a) and (b) shows the results from the CEM calculations for the $AGe_{1-x}Sn_xI_3$ and $APb_{1-x}Ge_xI_3$, which are the systems containing mixed divalent cations. The formation energies of symmetry-nonequivalent structures were calculated for 84, 96, and 65 atoms per supercell for $AGe_{1-x}Sn_xI_3$ (A = MA, FA, and Cs) and 96, 84, and 45 atoms per supercell for $APb_{1-x}Ge_xI_3$ (A = MA, FA, and Cs). $APbI_3$, $ASnI_3$, and $AGeI_3$ were used as the reference states for the estimation of the formation energies. For $AGe_{1-x}Sn_xI_3$, the characteristics are very similar to those of $APb_{1-x}Sn_xI_3$, such as the formation of a stable solid solution with A = Cs and an unstable solid solution with A = MA and FA, as shown in Figure 6(a). For $APb_{1-x}Ge_xI_3$, compounds containing Cs^+ and FA have slightly negative formation energies, suggesting that the solid solution is stable in this system. However, in the latter system, the energy gain seems to be very small relative to the system containing Cs^+. From these calculated results,

mixed divalent cations at the B site stabilize the perovskite structure for A = Cs^+ but destabilize it for A= MA and FA. The former result is caused by attractive interactions between the B-site ions, and the latter results are due to the relative weak attractive interaction between the B-site ions. The A-site dependence of the stability of perovskite structures has never been reported and is a fascinating property in organic–inorganic hybrid perovskites.

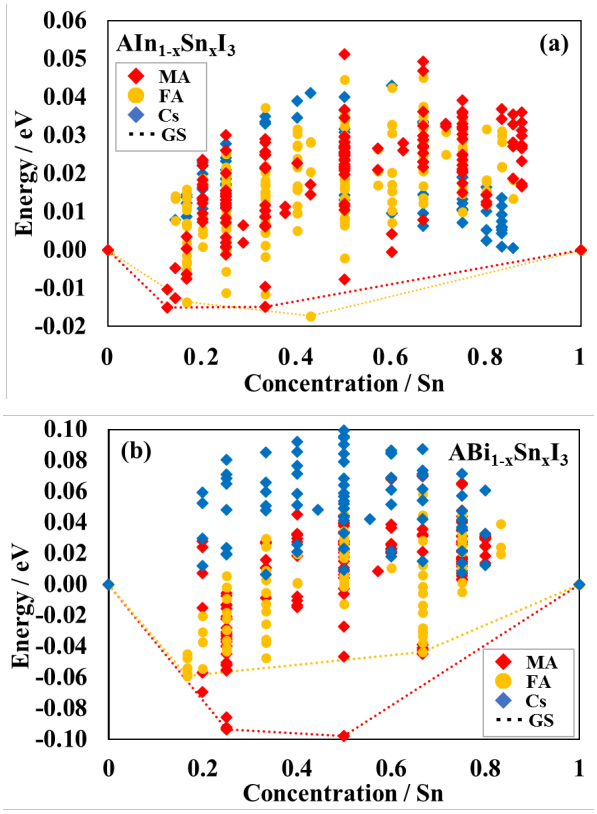

Figure 7. Results of ground state search performed using the CEM on (a) $AIn_{1-x}Sn_xI_3$ and (b) $ABi_{1-x}Sn_xI_3$.

On the other hand, the observed A-site dependence is not common in the iodide perovskite compounds. This behavior is completely reversed in several systems, for example, B = (In, Sn) and (Bi, Sn). Figures 7(a) and (b) show the results of the ground state search for the $AIn_{1-x}Sn_xI_3$ and $ABi_{1-x}Sn_xI_3$ systems, respectively. The formation energies of symmetry-nonequivalent structures were calculated for up to 96, 84, and 45 atoms per supercell for $AIn_{1-x}Sn_xI_3$ (A = MA, FA, and Cs^+) and 72, 72, and 60 atoms per supercell for $ABi_{1-x}Sn_xI_3$ (A = MA, FA, and Cs^+). $AInI_3$, $ASnI_3$, and $ABiI_3$ were used as the reference states for the estimation of the formation energies. In both systems, stable

structures were obtained in the cases of A = MA and FA. For the A = Cs^+ system, all the structures show positive formation energies, and we could not find stable structures, which have negative formation energies. This behavior is completely different from the results for $APb_{1-x}Sn_xI_3$, $AGe_{1-x}Sn_xI_3$, and $APb_{1-x}Ge_xI_3$. Similar behavior was also observed in the $A(Bi,Ge)I_3$ system (not shown).

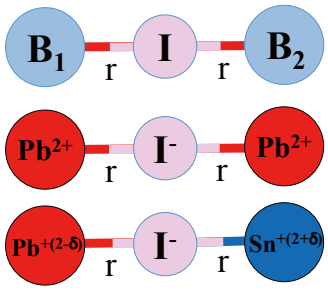

Figure 8. Model system (B_1—I—B_2 trimer) to show how charge transfer results in Coulomb energy gain by mixing B elements.

Concerning the origin of the stabilization of the perovskite structure in partially substituted systems, the difference in the energies of the pure perovskites and the partially substituted perovskites was considered. The energy difference between the pure perovskite and partially substituted system may originate from the lattice distortion and the charge disproportionation in the substituted system. The former contribution is always positive, which causes the system to become unstable. Therefore, the latter mechanism may result in the stabilization of the structure. Here, we consider the Coulomb energy gain, which is discussed in Ref. 20, at the X site, which arises because of the ionic bonding between the B-site cation and I, as shown in Figure 8. In the case of only one type B-site cation, the Coulomb energy, E_1, in the B_1-I-B_2 bonding configuration is given by Eq. (4).

$$E_1^{coul} = -\frac{2}{r} \tag{4}$$

Here, r is the distance between B and I. In the case of two types of B-site cation, the Coulomb energy, E_2, is given by Eq. (5).

$$E_2^{coul} = -\frac{\delta^2+4}{2r} \tag{5}$$

Here, δ is the difference between the charges at the B sites. The energy difference of the substituted system from the pure system is given by Eq. (6).

$$\Delta E^{coul} = E_2^{coul} - E_1^{coul} = -\frac{\delta^2}{2r} \quad (6)$$

Therefore, the Coulomb energy gain in the B-site substituted system is dependent on the difference in the charges, δ, at different B sites.

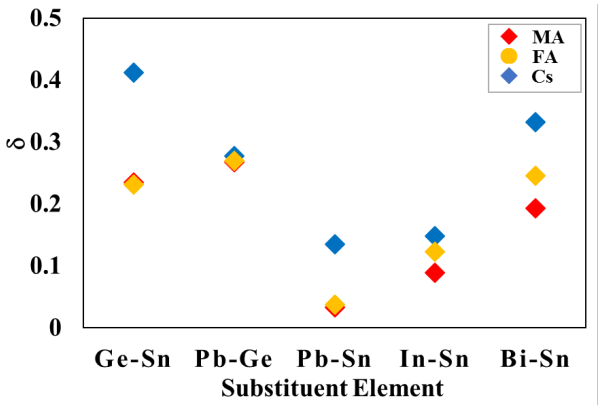

Figure 9. The difference in the charges (δ) at different B sites.

Based on the above considerations, the Coulomb energy gain was examined in terms of the difference in the charge, δ, at the B sites. As the difference in the electric charge, δ, increases, the Coulomb energy gain also increases. Figure 9 shows the B-site-ion dependence of δ for A = MA, FA, and Cs. For MA and FA, the δ values are smaller than those of the Cs compounds. Due to the small δ, the Coulomb energy gain is expected to be low for MA and FA. Therefore, the partially substituted structures are unstable. From these results, the partially substituted systems containing A = Cs are expected to be stabilized by the Coulomb energy gain. Therefore, new stable structures will be discovered in the partially substituted perovskite compounds with A = Cs or another inorganic element. Although the stable structures obtained in our study are possible candidates for solar cells, more studies are required to evaluate their suitability, such as the measurement of band gap, carrier mobility, and defect density in the future work.

On the other hand, the Coulomb energy gain mechanism for the stabilization of the partially substituted perovskite compounds cannot explain the results for the $AIn_{1-x}Sn_xI_3$ and $ABi_{1-x}Sn_xI_3$ systems. This drastic change in the stability of the perovskite compounds with the changing A-site is a surprising and interesting property, but the microscopic mechanism for this phenomenon is not clear at present. We speculate that an important factor for this behavior is the stable oxidation state of the B-site ions. In this study, Pb, Sn, Ge, In, and Bi were considered as B-site ions. Among of them, stable oxidation state of Pb, Sn, and Ge is +2 or +4, and In and Bi have other stable oxidation states, such as +3 or +5. In the former systems, the solid solutions are stabilized when A

= Cs^+, and, in the latter systems, the solid solutions are stabilized when A = MA and FA. From the simple consideration in terms of the ionic bonding, iodide perovskite compounds are stabilized by divalent B-site ions. Therefore, divalent cations Pb^{2+}, Sn^{2+}, and Ge^{2+} are plausible oxidation state in the perovskite compounds under a neutrality condition. On the other hand, the introduction of cations in different oxidation states, such as In and Bi, into the system will have a significant influence on the lattice distortion and the electronic state. To maintain charge neutrality in the unit cell, additional electrons introduced through In or Bi substitution are considered to extend in the unit cell. This may cause distortion and give a metallic (physical) property to the system. However, it is nontrivial to identify the electronic state of the B-site ions, except for divalent cations, in the perovskite compounds. Supposedly, it is not a typical ionic crystal but has a metallic-like bond with covalent bonding between neighboring ions. This issue must be determined in future work.

Conclusion

For the development of lead-free or lower-lead-content perovskite solar cells, the stabilities of iodide perovskite compounds where Pb is fully or partially substituted by other cations were investigated.

For the fully substituted system, ionic bonding was crucial for the stability of the perovskite structure. The ionic bonding between A and I is weakened when an organic molecule, such as MA or FA, is placed at the A site.

For the partially substituted systems, we employed the cluster expansion method for the ground state search in the solid solution $A(B,B')I_3$. For the A site, two kinds of organic molecules, MA and FA, and one inorganic ion, Cs, were considered, and we found that the stability of the partially substituted system $A(B,B')I_3$ strongly depends on the identity of the ion at the A-site. The result of the ground state search can be summarized as follows.

1. For the combinations of A = Cs^+ with Pb, Sn, and Ge, the formation energies are negative. An attractive interaction acts between the B-site ions, stabilizing the perovskite structure. On the other hand, the formation energies are positive for A = MA and FA, where there are relative weak attractive interaction between the B-site ions, destabilizing the perovskite structure.
2. For the systems with B = (In,Sn) and (Bi,Sn), the formation energies are negative for A = MA and FA, where there are attractive interactions between the B-site ions, stabilizing the perovskite structure. This behavior is the opposite of that of point 1.

In summary, $Cs(B,B')I_3$ structures are stabilized by a mixture of divalent cations, such as Pb, Sn, and Ge. On the other hand, $MA(B,B')I_3$, and $MA(B,B')I_3$ are stabilized by the combination of divalent and trivalent cations, such as the In-Sn and In-Bi systems.

The microscopic mechanism of the role of A-site ions on the structural stability has been studied in terms of the electronic state and bonding between each site. Because of the ionic bonding, the very different charges between the B and B' sites in the $A(B,B')I_3$ solid solution stabilize the perovskite structure by Coulomb interactions. The Coulomb energy gain seems to be a plausible mechanism for the stabilization of $Cs(B,B')I_3$ for B = Pb, Sn, and Ge. Thus, the Coulomb energy gain is expected to be a guiding principle in the search for new partially substituted perovskite compounds.

Supporting Information

DFT calculation data of ABI_3 and the partially substituted system $A(B,B')I_3$, formation energies, crystallographic data, band gap, and the relaxed structures.

Acknowledgement

This paper is based on results partly obtained from a project subsidized by the New Energy and Industrial Technology Development Organization (NEDO).

References

[1] Kojima, A.; Teshima, K.; Shirai, Y.; Miyasaka, T. Organometal halide perovskites as visible-light sensitizers for photovoltaic cells. *J. Am. Chem. Soc.* **2009,** 131, 6050–6051.

[2] See https://www.nrel.gov/pv/assets/images/efficiency-chart.png for NREL efficiency chart.

[3] Noh, J. H.; Im, S. H.; Heo, J. H.; Mandal, T. N.; Seok, S. Chemical management for colorful, efficient, and stable inorganic-organic hybrid nanostructured solar cells. *Nano Lett.* **2013,** 13, 1764–1769.

[4] Stoumpos, C. C.; Malliakas, C. D.; Kanatzidis, M. G. Semiconducting tin and lead iodide perovskites with organic cations: phase transitions, high mobilities, and near-infrared photoluminescent properties. *Inorg. Chem.* **2013,** 52, 9019–9038.

[5] Niu, G.; Guo, X.; Wang, L. Review of recent progress in chemical stability of perovskite solar cells. *J. Mater. Chem.* A **2015,** 3, 8970–8980.

[6] Bernal, C.; Yang, K. First-principles hybrid functional study of the organic–inorganic perovskites $CH_3NH_3SnBr_3$ and $CH_3NH_3SnI_3$. *J. Phys. Chem.* C **2014,** 118, 24383–24388.

[7] Umari, P.; Mosconi, E.; Angelis, F. D. Relativistic GW calculations on $CH_3NH_3PbI_3$ and $CH_3NH_3SnI_3$ perovskites for solar cell applications. *Sci. Rep.* **2014,** 4, 4467.

[8] Xu, P.; Chen, S.; Xiang, H.-J.; Gong, X.-G.; Wei, S.-H. Influence of defects and synthesis conditions on the photovoltaic performance of perovskite semiconductor $CsSnI_3$. *Chem. Mater.* **2014,** 26, 6068–6072.

[9] Jacobsson, T. J.; Pazoki, M.; Hagfeldt, A.; Edvinsson, T. Goldschmidt's rules and strontium replacement in lead halogen perovskite solar cells: theory and preliminary experiments on $CH_3NH_3SrI_3$. *J. Phys. Chem.* C **2015,** 119, 25673–25683.

[10] Sun, Y.-Y.; Shi, J.; Lian, J.; Gao, W.; Agiorgousis, M. L.; Zhang, P.; Zhang, S. Discovering lead-free perovskite solar materials with a split-anion approach. *Nanoscale* **2016,** 8, 6284–6289.

[11] Giorgi, G.; Yamashita, K. Alternative, lead-free, hybrid organic–inorganic perovskites for solar applications: a DFT analysis. *Chem. Lett.* **2015,** 44, 6, 826–828.

[12] Uribe, J. I.; Ramirez, D.; Osorio-Guillén, J. M.; Osorio, J.; Jaramillo, F. $CH_3NH_3CaI_3$ perovskite: synthesis, characterization, and first-principles studies. *J. Phys. Chem.* C **2016**, 120, 16393–16398.

[13] Sun, Y. Y.; Agiorgousis, M. L.; Zhang, P.; Zhang, S. Chalcogenide perovskites for photovoltaics. *Nano Lett.* **2015,** 15, 581–585.

[14] Brivio, F.; Butler, K. T.; Walsh, A.; Relativistic quasiparticle self-consistent electronic structure of hybrid halide perovskite photovoltaic absorbers. *Phys. Rev.* B **2014**, 89, 155204.

[15] Brgoch, J.; Lehner, A. J.; Chabinyc, M.; Seshadri, R. Ab initio calculations of band gaps and absolute band positions of polymorphs of $RbPbI_3$ and $CsPbI_3$: implications for main-group halide perovskite photovoltaics. *J. Phys. Chem.* C **2014**, 118, 27721–27727.

[16] Volonakis, G.; Filip, M. R.; Haghighirad, A. A.; Sakai, N.; Wenger, B. Lead-free halide double perovskites via heterovalent substitution of noble metals, *J. Phys. Chem. Lett.* **2016,** 7, 1254–1259.

[17] Zhao, X.-G.; Yang, D.; Sun, Y.; Li, T.; Zhang, L.; Yu, L.; Zunger, A. Cu–In halide perovskite solar absorbers. *J. Am. Chem. Soc.* **2017**, 139, 6718–6725.

[18] Zhao, X.-G.; Yang, J.-H.; Fu, Y.; Yang, D.; Xu, Q.; Yu, L.; Wei, S.-H.; Zhang, L. Design of lead-free inorganic halide perovskites for solar cells via cation-transmutation. *J. Am. Chem. Soc.* **2017**, 139, 2630–2638.

[19] Savory, C. N.; Walsh, A.; Scanlon, D. O. Can Pb-free halide double perovskites support high-efficiency solar cells? *ACS Energy Lett.* **2016**, 1, 949–955.

[20] Yin, W.-J.; Yan, Y.; Wei, S.-H. Anomalous alloy properties in mixed halide perovskites. *J. Phys. Chem. Lett.* **2014**, 5, 3625–3631.

[21] van de Walle, A.; Asta, M.; Ceder, G. The alloy theoretic automated toolkit: A user

guide. *CALPHAD* **2002**, 26, 539–553.

[22] Sanchez, J. M.; Ducastelle, F.; Gratias, D. Generalized cluster description of multicomponent systems. *Physica* A **1984**, 128, 334–350.

[23] Sanchez, J. M.; Becker, J. D. Phase stability and diagrams from first principles. *Mater. Res. Soc. Symp. Proc.* **1993**, 291, 115–127.

[24] de Fontaine, D. *Solid State Physics*, Academic Press: New York, **1994**.

[25] Sluiter, M.H.F.; Watanabe, Y.; de Fontaine, D.; Kawazoe, Y. First-principles calculation of the pressure dependence of phase equilibria in the Al-Li system. *Phys. Rev.* B **1996**, 53, 6137–6151.

[26] Kresse, G.; Furthmüller, J. Efficient iterative schemes for ab initio total-energy calculations using a plane-wave basis set. *Phys. Rev.* B, **1996**, 54, 11169–11186.

[27] Kresse, G.; Furthmüller, J. Efficiency of ab-initio total energy calculations for metals and semiconductors using a plane-wave basis set. *Comput. Mater. Sci.* **1996**, 6, 15–50.

[28] Perdew, J. P.; Burke, K.; Ernzerhof, M. Generalized gradient approximation made simple. *Phys. Rev. Lett.* **1996**, 77, 3865–3868.

[29] Kresse, G.; Joubert, D.; From ultrasoft pseudopotentials to the projector augmented-wave method. *Phys. Rev.* B **1999**, 59, 1758.

[30] Tang, W.; Sanville, E.; Henkelman, G. A grid-based Bader analysis algorithm without lattice bias. *J. Phys.: Condens. Matter* **2009**, 21, 084204.

[31] Koh, T. M.; Fu, K.; Fang, Y.; Chen, S.; Sum, T. C.; Mathews, N.; Mhaisalkar, S. G.; Boix, P. P.; Baikie, T. Formamidinium-containing metal-halide: an alternative material for near-IR absorption perovskite solar cells. *J. Phys. Chem.* C **2014**, 118, 16458–16462.

[32] Eperon, G. E.; Stranks, S. D.; Menelaou, C.; Johnston, M. B.; Herz, L. M.; Snaith, H. J. Formamidinium lead trihalide: a broadly tunable perovskite for efficient planar heterojunction solar cells. *Energy Environ. Sci.* **2014**, 7, 982–988.

[33] Beal, R. E.; Slotcavage, D. J.; Leijtens, T.; Bowring, A. R.; Belisle, R. A.; Nguyen, W. H.; Burkhard, G. F.; Hoke, E. T.; McGehee, M. D. Cesium lead halide perovskites with improved stability for tandem solar cells. *J. Phys. Chem. Lett.* **2016**, 7, 746–751.

[34] Tani, Y.; Sato, K.; Katayama-Yoshida, H. Materials design of spinodal nanodecomposition in $CuIn_{1-x}Ga_xSe_2$ for high-efficiency solar energy conversion. *Applied Physics Express* **2010**, 3, 101201.

TOC Graphic

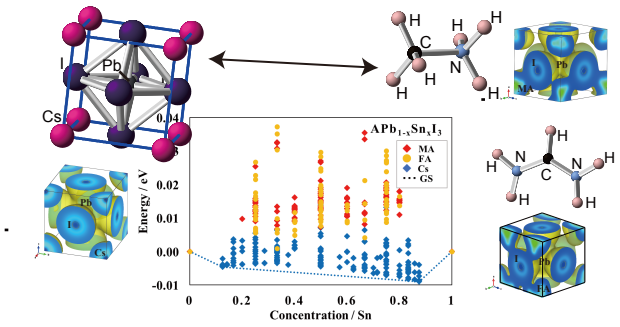
Pb
I
Cs
H
C
N
MA
APb1-xSnxI3
MA
FA
Cs
GS
Energy / eV
0.02
0.01
0.00
-0.01
0
0.2
0.4
0.6
0.8
1
Concentration / Sn